ECS Transactions, 72 (23) 31-51 (2016)
10.1149/07223.0031ecst ©The Electrochemical Society

Thin film Catalysts: Ni_5P_4 (Cathodic) and $LiCoO_2$ (Anodic) for Electrolysis of Water

S. Hwang[a,b,#], S. H. Porter[a,b,#], G. Gardner[a,b], A. B. Laursen[a,b], H. Wang[a,c], M. Li[a,b], V. Amarasinghe[b,c], E. Taghaddos[d], A. Safari[d], E. Garfunkel[a,b], M. Greenblatt[a,b], and G. C. Dismukes[a,b,*]

[a] Institute for Advanced Materials, Devices, and Nanotechnology, Rutgers University, New Brunswick, New Jersey 08854, USA
[b] Department of Chemistry & Chemical Biology, Rutgers University, New Brunswick, New Jersey, 08854, USA
[c] Department of Physics & Astronomy, Rutgers University, New Brunswick, New Jersey, 08854, USA
[d] Department of Materials Science and Engineering, Rutgers University, New Brunswick, New Jersey, 08854, USA
[#] These authors contributed equally to this work, [*] To whom correspondence should be addressed

Inexpensive earth-abundant catalysts are required to accelerate both the oxidative and reductive half reactions for electrolysis of water. Using natural enzymes as models, such as the $CaMn_4O_5$ cubane motif in the water oxidizing complex of photosystem II and the Ni-S active site of Ni-Fe hydrogenase, we previously developed cubic $LiCoO_2$ (1) and nickel phosphides that mimic their chemistry, respectively (2). Here we prepared thin films of spinel – $LiCo_2O_4$, for the (water oxidation) oxygen evolving reaction (OER), and Ni_5P_4, for the hydrogen evolving reaction (HER) on Au substrates. We investigated their atomic structure (PXRD), Raman vibrational modes, surface morphology (SEM, AFM), core electronic levels (XPS), and electrochemical catalytic performance. These non-precious metal thin film materials function as well as the individual nanocrystalline particles and are expected to be applicable to use in monolithic photoelectrochemical cells and potentially fuel cells.

Introduction

Water splitting into hydrogen and oxygen using sun light is a promising method to harvest and store energy (3). Among different strategies to split water, the photoelectrochemical cell (PEC) is attractive due to high theoretical solar to hydrogen efficiencies (12-22%, depending on configuration) (4). However, splitting of water requires high thermodynamic energy (237 kJ/mol) and must overcome high activation energy barriers for both oxygen and hydrogen evolution, which compel the need for active electrocatalysts. Recently, many electrocatalysts for both OER and HER with earth abundant metal oxides or metal phosphides have been developed to replace non-scalable platinum group metals (5-9). In an integrated PEC where the catalyst also serves to create a buried junction for a semiconductor photoabsorber, it is essential to form conformal,

stable, thin films (< 30nm) of catalyst that are maximally transparent and active. Few metal oxide, or metal phosphide catalysts have achieved this feat.

Many researchers have heavily studied first-row transition metal oxides and oxyhydroxides, especially Fe-, Co-, and Ni-based heterogeneous catalysts due to their comparable overpotential with the precious metal catalysts (10-12). Our group has extensively studied $LiCoO_2$, since we first discovered that while layered $LiCoO_2$ ($R\bar{3}m$) is inactive, cubic-$LiCoO_2$ ($Fd\bar{3}m$) shows high OER activity near neutral pH using a photochemically driven system (1). Only cubic-$LiCoO_2$ contains $[Co_4O_4]^{n+}$ cubic subunits, which are a close analogue of the $[CaMn_3O_4]^{n+}$ in the water oxidation complex of Photosystem II, and provides low overpotential for the formation of Co^{4+} as well as low intercubane hole mobility (13). Further studies recently showed that cubic-$LiCoO_2$ has better OER performance than platinum group metals when applied as an anode (Pt cathode) in an anion exchange membrane (AEM) electrolyzer. It was also demonstrated that this catalyst is stable at high current density (> 100 mA/cm^2) over long intervals (>1000 hours) (13).

Transition metal phosphides (TMP) have gained much attention as electrocatalysts for HER because of their exceptional activity among non-platinum group catalysts (2,14-15). Our group recently established that micron size particles of crystalline Ni_5P_4 (Ni_5P_4 MP) has comparable overpotential with Pt foil at 10 mA/cm^2 (geometric based) (2) and that Ni_5P_4 MP is stable in both acidic and basic media (2). Although the synthesis of micrometer thick films of layered $LiCoO_2$ (16) or Ni_2P (17) have been published, sub-hundred nanometer thin films of cubic-$LiCoO_2$ (or spinel phase) and Ni_5P_4 for overall water electrolysis has not yet been demonstrated. Herein, we report the fabrication of conformal thin films of $LiCoO_2$ OER and Ni_5P_4 HER electrocatalysts on conductive substrates with excellent activity and stability.

Experimental

Chemicals

$NiCl_2$ (Mathson Coleman & Bell, >98%), $NiSO_4$•$6H_2O$ (Sigma Aldrich, 99%), H_3PO_4 (Sigma Aldrich, >85%), NaH_2PO_2•H_2O (Sigma Aldrich, >99%), $LiNO_3$(Sigma Aldrich, >98%), $Co(NO_3)_2$•$6H_2O$ (Sigma Aldrich, 98%), citric acid (Sigma Aldrich, 99%), urea (Sigma Aldrich, 99.0-100.5%), and NaOH (Sigma Aldrich, 98%) were used as received. The substrates used were 100 nm Au (including Cr adhesive layer) coated on borosilicate glass.

PLD target preparation

Sol-gel methods (1) were adopted to prepare a pulsed laser deposition (PLD) target. Aqueous $LiNO_3$, $Co(NO_3)_2$•$6H_2O$, citric acid and urea (1:1 Li to Co stoichiometry with excess citric acid and urea) was evaporated at 80 ºC for 6 h, and then further evaporated at 170 ºC for 12h. The resulting precursor powder was then ground and decomposed at 450 ºC for 6h. A layered $LiCoO_2$ product was confirmed by powder X-ray diffraction (PXRD), before uni-axially pressing it into a pellet at 105 MPa. The pressed pellet was further sintered at 780 ºC for 24h for densification. The target measured 90% of theoretical density.

PLD deposition of $LiCoO_2$

Thin films of $LiCoO_2$ were deposited by the PLD method, with a standard configuration used (18). The distance from target to the substrate was fixed at 7 cm. Thin films of $LiCoO_2$ were deposited on Au coated glass substrate. The PLD chamber was evacuated to the base pressure of 5-9x10^{-6} Torr and then backfilled with 1 Torr of ultra-high purity of oxygen. A laser bombardment reaction was made with a KrF laser (248 nm). The fluence per pulse was 2.5 - to - 3 J/cm^2 with deposition at 450 ºC for 20 min.

Electrochemical deposition of Ni_5P_4

Thin films of Ni_5P_4 were fabricated by electrochemical deposition, followed by a solvothermal annealing. Electrochemical depositions were conducted in a 100 ml three-neck round bottom flask in a 0.75 M $NiSO_4$•$6H_2O$, 0.25 M $NiCl_2$•$6H_2O$, 1.75 M NaH_2PO_2•H_2O, and 0.5 M H_3PO_4 solution; the pH was adjusted to 3 by addition of NaOH. Working electrodes were prepared from Au coated glass by front-side contact where Cu wire is Cu taped as a lead and then this area is sealed from electrolyte exposure with Teflon adhesive tape or epoxy. Pt foil was used as counter electrode, which was separated from the main compartment by a Selemion (Asahi Glass, Japan) anion exchange membrane, preventing dissolution and re-deposition of Pt on the working electrode during electrochemical deposition (19). Ag/AgCl in 3.5 M KCl was used as a reference electrode. All deposition solutions were purged by Ar for at least 30 min before commencing deposition. Cyclic voltammetry techniques were used for determination of deposition potential for both Ni and P. At 0.7 V vs. RHE nickel phosphides begin to form, with Ni/P ratios decreasing at higher potential. However, at greater than 1.1 V vs. RHE, H_2 bubble formation is so intense during deposition (HER is a side reaction), that deposited (amorphous) Ni-P film quality degrades. Therefore, thin film deposition at 1 V vs. RHE was selected with the potentio-pulse method (20), which enables precise control of film thickness. The nickel phosphide films were crystallized by solvothermal annealing (2): briefly, 2 mL trioctylphosphine (TOP) and 2 g of trioctylphosphine oxide (TOPO) were placed together with the electrodeposited film in a round bottom flask. The flask was connected to a condenser in one port, N_2 purging line in the other, and a glass tube with thermocouple probe in the third. The condenser was connected to a silicone oil bubbler, which was vented into a fume hood. The reaction flask was well sealed and purged with flowing N_2 (200 mL/min) before annealing was started; then the N_2 flow was adjusted to 25 mL/min and the flask was placed into a preheated sand bath at 450 ºC; the solution temperature during annealing was 320-330 ºC for 1.5 h.

Characterization techniques

Powder X-ray diffraction (PXRD) was carried out on a Bruker (Billerica, MA, USA) D8 Advance (Cu Kα1, 0.02° step size, 10-15 sec dwell time). Helium ion microscopy (HeIM) with a Carl Zeiss (Oberkochen, Germany) ORION PLUS SHIM was operated at 30kV for all imaging. Top-view of film morphologies were observed by scanning electron microscopy (Zeiss Sigma Field Emission SEM with Oxford EDSLEO FESEM). For X-ray photoelectron spectroscopy measurements, Thermo (Waltham, MA) K- Alpha spectrometer was used with charge compensation; spectra were calibrated against adventitious carbon. Atomic force microscopy (AFM) images were generated using a

Park Systems (Suwon, Korea) NX-10 with a Nanosensors (Neuchatel, Switzerland) PPP-NCHR tip in electrostatic force mode at room temperature in air.

Electrochemical measurements

Prior to measurements, the glassware was cleaned with piranha solution followed by rinsing with copious amount of deionized water. Standard electrochemical procedures were carried out with an Ametek (Berwyn, PA, USA) VERSASTAT3 (for electrodeposition), a PARSTAT 2263 potentiostat (for HER), and a CH Instrument (Austin, TX, USA) Electrochemical Workstation (for OER). The electrolyte was purged with H_2 (HER) or Ar (OER or full cell) for 10 min prior to measurements. For half-cell measurements (HER or OER), standard 3 electrode configuration was used in 1M NaOH with a 1x1cm boron-doped CVD diamond counter electrode and an Ag/AgCl reference electrode. For full cell measurements, a standard 2 electrode configuration was used with all the same parameters as the 3-electrode set-up, except the reference electrode was removed.

Results and discussion

Structural and surface characterization of thin film $LiCoO_2$

The as-synthesized crystalline PXRD of cubic-$LiCoO_2$ are well matched with the reference patterns (Figure 1A), confirming phase pure product for the PLD target. High density is important for PLD target, because a low density target can lead to micro size agglomeration on film (21). High temperature sintering resulted in a phase transformation to layered $LiCoO_2$ (Figure 1B), which was used for thin film deposition.

The $LiCoO_2$ thin film deposited on the Au substrate reveals one Bragg reflection related to $LiCoO_2$, which indicates epitaxial growth of films. The identification of phase by PXRD peak position, however, is ambiguous because the peaks overlap with those of the Au substrate. Moreover, the single peak of $LiCoO_2$ is broad and appears to be intermediate between the cubic and layered $LiCoO_2$ peaks at 18.9 and 19.2°2θ (Figure 2). Since the Au substrate is (111) oriented, the synthesized film might be fully, or partially oriented on the substrate (5). Raman spectroscopy can be used to definitively determine between the two different $LiCoO_2$ phases, because the layered structure ($R\bar{3}m$) has two Raman active modes (E_g, and A_{1g}), while cubic or spinel ($Fd\bar{3}m$) has four different Raman active modes (E_g, A_{1g}, and $2F_{2g}$) (22). The PLD prepared samples indicated two Raman active modes at 486 cm^{-1}, and 592 cm^{-1}, corresponding to layered $LiCoO_2$ (Figure 3). However, recently, our group found that under OER electrolysis condition in basic media, both cubic and layered phases of $LiCoO_2$ will have partial de-intercalation of labile lithium resulting in a structural reorganization to cubic spinel structure, which is the OER active form (13). For confirmation of reorganization, we examined the Raman spectra of a sample of $LiCo_2O_4$ film after post electrolysis in basic media: of the expected four different Raman active modes ($2F_{2g}$, E_g, A_{1g}) of spinel $LiCo_2O_4$ (23), Raman shifts at 481, 616, and 687 cm^{-1} (Figure 3), corresponding to F_{2g}, E_g, A_{1g}, indicate structure reorganization during (or post) OER electrolysis. Nevertheless the Raman shift at 586 cm^{-1} ascribed to the layered phase, and the absence of 525 cm^{-1} (F_{2g}) Raman suggest only

partial structure reorganization. Due to the thin film characteristic and de-lithiation process during OER electrolysis, all Raman shifts of post OER electrolysis samples showed peak broadening. Raman analysis suggests that our thin film of $LiCoO_2$ changes structure to the cubic polymorph following OER activity.

Characterization of the physical properties of the prepared films is required to account for and understand surface area, coverage, and mechanical stability, which also give context for electrode fabrication, as well as the electrochemical performance. The deposited $LiCoO_2$ thin film had conformal coverage on the Au substrate (Figure 4A), with a thickness of 30 nm (Figure 4B). The cross-section of the film was not well cleaved due to mechanical dicing that resulted in partial coverage of the $LiCoO_2$ layer by the Au substrate. Roughness is another important characteristic of the active film for heterogeneous catalysis, as it can vary the surface active sites for the reaction, and thus change catalytic activity (24). Roughness of the synthesized thin film is 11.8 nm (Figure 6A).

Since PLD can be a harsh process and Li can suffer from volatilization, it is important to verify whether or not Li is completely incorporated during thin film deposition. The Li 1s core level spectrum (Figure 5A) with peak binding at 54.21 eV corresponds to lattice Li in $LiCoO_2$ (25), confirming its presence in the prepared samples. Aside from lithium content, the activity of a cobalt-containing OER catalyst is sensitive to the oxidation state of Co (26). Determination of oxidation state of Co can detect a possible Co_3O_4 secondary phase, which contains less anti-corrosive Co^{2+} species that prevent long term stability under OER operating conditions (27). The synthesized thin film of $LiCoO_2$ was compared to a reference Co_3O_4 powder (Alfa Aesar) (Figure 5B). The cobalt XPS spectrum consisted of two spin-orbit coupling peaks ($2p_{3/2}$ and $2p_{2/1}$) and two satellite peaks, which can be used for the determination of Co^{2+} and Co^{3+} oxidation states. Binding energies at 790 eV and 805 eV correspond to Co^{3+}, whereas binding energy 786 eV and 803 eV are Co^{2+}. Co_3O_4 has 1:2 ratio of Co^{2+}: Co^{3+} species, which gave four satellite peaks (28). Co_3O_4 has intensity at 786 eV, while in $LiCoO_2$ this feature is nearly unresolved from the background (Figure 5B), demonstrating that the thin film of $LiCoO_2$ has only Co^{3+} species present.

OER activity and stability of thin film $LiCoO_2$

The IR-corrected cyclic voltammogram indicate that 420 mV overpotential (1.65V vs. RHE) is required to maintain a current density of 10 mA/cm^2 (Figure 7) during water oxidation. The Tafel slope is 57 mV/dec. Both overpotential and Tafel slope are well matched with previously reported $LiCoO_2$ powder samples (12). These values demonstrate excellent OER activity for the $LiCoO_2$ thin film given that electrodes are flat and of low surface area.

The thin films are stable post-electrolysis. No significant change in cell potential is observed after electrolysis of water at 10 mA/cm^2 for 12 h (Figure 8A). The cyclic voltammogram was not significantly changed and has required similar overpotential (430 mV final versus 420mV initial) to drive 10 mA/cm^2 (Figure 7). Furthermore, the Tafel slope remained the same as well (56 mV/decade final vs 57mV/decade initial). The post electrolysis films had negligible change in surface roughness (R_a = 12.2 nm final versus 11.8 nm initial; Figure 6B). Electronically, there were no changes in the oxidation state of

cobalt (Figure 8). Lastly, there was no evidence for dissolution of the films in the electrolyte per unit time, confirmed by inductively coupled plasma optical emission spectroscopy of the electrolyte of post-electrolysis. These results confirm that a thin film spinel $LiCo_2O_4$ has been formed that mimics the pressed pellet fabricated from bulk powder, with regard to electrochemical stability and activity for OER.

Structural and surface characterization of thin film Ni_5P_4

The as-deposited films homogenously covered the substrate and had a smooth surface (Figure 9A). The roughness (R_a) of the films is only 1.7 nm (Figure 9B), which indicates an extremely flat surface. To crystallize the films, a post-annealing step was conducted. The PXRD of the annealed films indicates that although the Au (111) substrate signal overlaps with some of the Ni_5P_4 peaks between 30-40º 2θ (Figure 11A), in the range 40-60º the PXRD of deposited Ni_5P_4 film matches well with that of the Ni_5P_4 reference diffraction pattern (Figure 11B). To confirm that there was no leaching or incorporation of extra phosphorus during the solvothermal annealing step, post-reaction elemental analysis was carried out. The films were well covered with nickel and phosphorous and the Ni/P ratio was 1.02 (Figure 10A). This value, slightly lower than the theoretical value of 1.25 for Ni_5P_4, indicates that the post-annealing step produces a high phosphorous content on the top surface of the film via decomposition of the organic phosphorous solvothermal reactants. Confirming this observation, the surface sensitive technique, XPS, indicates a Ni/P ratio of 0.2, which is much lower than 1.02 for bulk. The SEM cross-section image demonstrates that the deposited film has thickness of 15 to 30 nm Ni_5P_4 (Figure 10B). Even though these Ni_5P_4 films are thin, they have conformal coating. The small irregular top surface features are a result of the solvothermally deposited phosphorus-rich top layer.

HER activity and stability of thin film Ni_5P_4

The HER activity of Ni_5P_4 thin films were demonstrated by IR-corrected averaged cyclic voltammogram (Figure 11A). The overpotential required for driving a current density of 10 mA/cm^2 is 330 mV, which, for a conformal thin film catalyst in basic solution is a promising value. There are limited reports of thin film transition metal phosphide HER catalysts in base. For corollary in acid, Hellestern *et al.* reported a 7.4 nm thin CoP film on n^+Si, which required 202 mV overpotential to drive the HER at 10 mA/cm^2 (15). The Tafel slope of thin film Ni_5P_4 is 98 mV/dec, which is the same as the pressed powder sample in 1M NaOH (16). The exchange current density is 3.16×10^{-6} A/cm^2. The stability of thin films examined at -10 mA/cm^2 with chronopotentiometry techniques, indicated that the overpotential was not significantly changed over 5 h of water reduction (Figure 11B). We conclude that the prepared thin films of Ni_5P_4 are HER active and stable in 1M NaOH.

Overall water splitting by Ni_5P_4 and $LiCoO_2$

The promising results of each half-cell warranted investigation of the full cell overpotentials, with a thin Ni_5P_4 film as the cathode and a thin $LiCoO_2$ film as the anode. The cathode Ni_5P_4 electrodes used for overall water splitting were about 100 nm thick while the $LiCoO_2$ electrode was 30 nm thick. Ni_5P_4 films produced that were thinner than 30 nm were not stable. Ongoing work is focused on understanding why this is so.

Averaged cyclic voltammograms for the full cell at 10 mA/cm^2 is achieved at a cell voltage of 1.86 V, which corresponds to 630 mV of overpotential required for water electrolysis (Figure 12A). The stability of the cell was investigated after 12 hours of chronopotentiometric electrolysis at 10 mA/cm^2. The cell voltage slightly increased over time (1.86 V initial to 1.98 V final cell voltage), but shows good stability over the duration of the experiment (Figure 12B). Durability studies at longer time scales are underway.

Conclusion

In summary, active $LiCo_2O_4$ OER and Ni_5P_4 HER catalysts as thin films have been made and examined with respect to their structure and catalytic properties. The films of both materials have the desired structural phase required for high activity water electrolysis. Fabricated films less than 30 nm thick, are still active for both OER and HER reaction in basic media (1M NaOH). Furthermore, the activity of the $LiCo_2O_4$ OER catalyst film is equivalent to that reported for pressed pellets of the nanocrystalline material. The Ni_5P_4 HER thin film, has promising activity when compared to the limited number of thin film catalysts that are stable in basic solution. This work demonstrates the retention of the superior catalytic performance of current state-of-the-art non-precious-metal catalysts when applied as thin film materials suitable for (photo)electrochemical applications.

Acknowledgments

Funding for this research was provided by a DOE/NSF grant: CBET-1433492.

References

1. G. P. Gardner, Y. B. Go, D. M. Robinson, P. F. Smith, J. Hadermann, A. Abakumov, M. Greenblatt, G. C. Dismukes, *Angew. Chem. Int. Ed.* **51**, 161 (2012).
2. A. B. Laursen, K. R. Patraju, M. J. Whitaker, M. Retuerto, T. Sarkar, N. Yao, K. V. Ramanujachary, M. Greenblatt, G. C. Dismukes, *Energy Environ. Sci.* **8**, 1027 (2015).
3. J. H. Kim, Y. Jo, J. H. Kim, J. H. Kim, J. W. Jang, H. J. Kang, Y. H. Lee, D. S. Kim, Y. Jun, J. S. Lee, *ACS Nano,* **9**, 11820 (2015).
4. M. S. D Prévot, K. Sivula, *J. Phys. Chem. C* ,**117**, 17879 (2013).
5. J. A. Koza, Z. He, A. S. Miller, J. A. Switzer, *Chem. Mater.*, **24**, 3567 (2012).
6. J. D. Blakemore, H. B. Gray, J. R. Winkler, A. M. Müller, *ACS Catal.*, **3**, 2497 (2013).
7. J. Tian, Q. Liu, A. M. Asiri, X. Sun, *J. Am. Chem. Soc.,* **136**, 7587 (2014).
8. X. Chen, D. Wang, Z. Wang, P. Zhou, Z. Wu, F. Jiang, *Chem. Commun.*, **50**, 11683 (2014).
9. Z. Xing, Q. Liu, A. M. Asiri, X. Sun, *ACS Catal.*, *5*, 145 (2014).
10. A. S. Batchellor, S. W. Boettcher, *ACS Catal.*, *5*, 6680 (2015).
11. A. M. Smith, L. Trotochaud, M. S. Burke, S. W. Boettcher, *Chem. Commun.,* **51**, 5261 (2015).
12. H. Liu, Y. Zhou, R. Moré, R. Müller, T. Fox, G. R. Patzke, *ACS Catal.*, **5**, 3791 (2015).

13. G. Gardner, J. Al-Sharab, N. Danilovic, Y. B. Go, K. Ayers, M. Greenblatt, G. C. Dismukes, *Energy Environ. Sci.*, **9**, 184 (2016).
14. Da Li, K. Senevirathne, L. Aquilina, S. L. Brock, *Inorg. Chem.*, **54**, 7968 (2015).
15. T. R. Hellstern, J. D. Benck, J. Kibsgaard, C. Hahn, T. F. Jaramillo, *Adv. Energy Mat.*, 1501758 (2015).
16. M. Antaya, K. Cearns, J. S. Preston, J. N. Reimers, J. R. Dahn, *J. Appl. Phys*., **76**, 2799 (1994).
17. E. J. Popczun, J. R. McKone, C. G. Read, A. J. Biacchi, A. M. Wiltrout, N. S. Lewis, and R. E. Schaak *J. Am. Chem. Soc.*, **135**, 9267 (2013).
18. M. M. Hejazi, E. Taghaddos, A. Safari, *J Mater Sci*., **48**, 3511 (2013).
19. S. Cherevko, A. R. Zeradjanin, G. P. Keeley, K. J. J. Mayrhofer, *J. Electrochem. Soc.*, **161**, H822 (2014).
20. S. A. Lajevardi, T. Shahrabi, *Appl. Surf. Sci*., **256**, 6775 (2010).
21. J.-H. Kim, S. Lee, H.-S. Im, *Appl. Surf. Sci*., **151**, 6 (1996).
22. L. Mendoza, R. Baddour-Hadjean, M. Cassir, J. P. Pereira-Ramos, *Appl. Surf. Sci.*, **225**, 356 (2004).
23. S. W. Song, K.-S. Han, M. Yoshimura, *J. Am. Ceram. Soc.,* **83**, 2839 (2000).
24. Y.-C. Liu, J. A. Koza, J. A. Switzer, *Electrochim. Acta*, **140**, 359 (2014).
25. K. Mukai, Y. Aoki, D. Andreica, A. Amato, I. Watanabe, S. R. Giblin, J. Sugiyama, *Phys. Rev. B*, **89**, 094406 (2014).
26. X. Deng, and, H. Tüysüz, *ACS Catal.*, **4**, 3701 (2014).
27. J. B. Gerken, J. G. McAlpin, J. Y. C. Chen, M. L. Rigsby, W. H. Casey, R. D. Britt, S. S. Stahl, *J. Am. Chem. Soc.*, **133**, 14431 (2011).
28. J. Yang, H. Liu, W. N. Martens, R. L. Frost, *J. Phys. Chem. C*., **114**, 111 (2009).

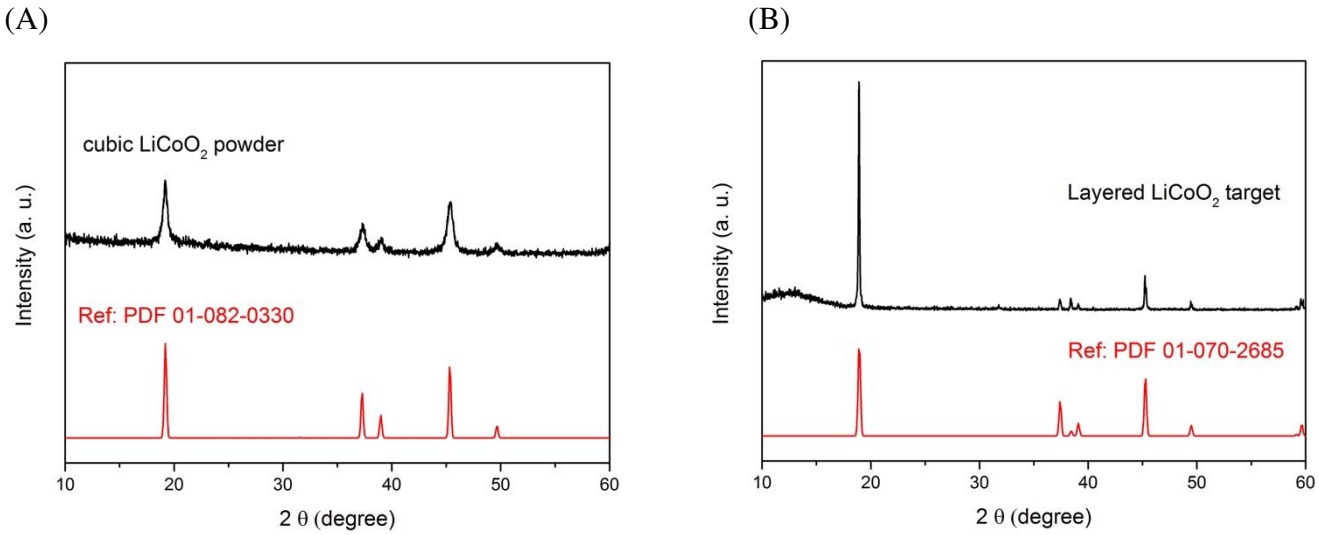

Figure 1. A) X-ray diffraction pattern of the bulk $LiCoO_2$ powder referenced against cubic (low temperature phase) $LiCoO_2$ and B) the as-prepared sintered target versus layered $LiCoO_2$ (high temperature phase).

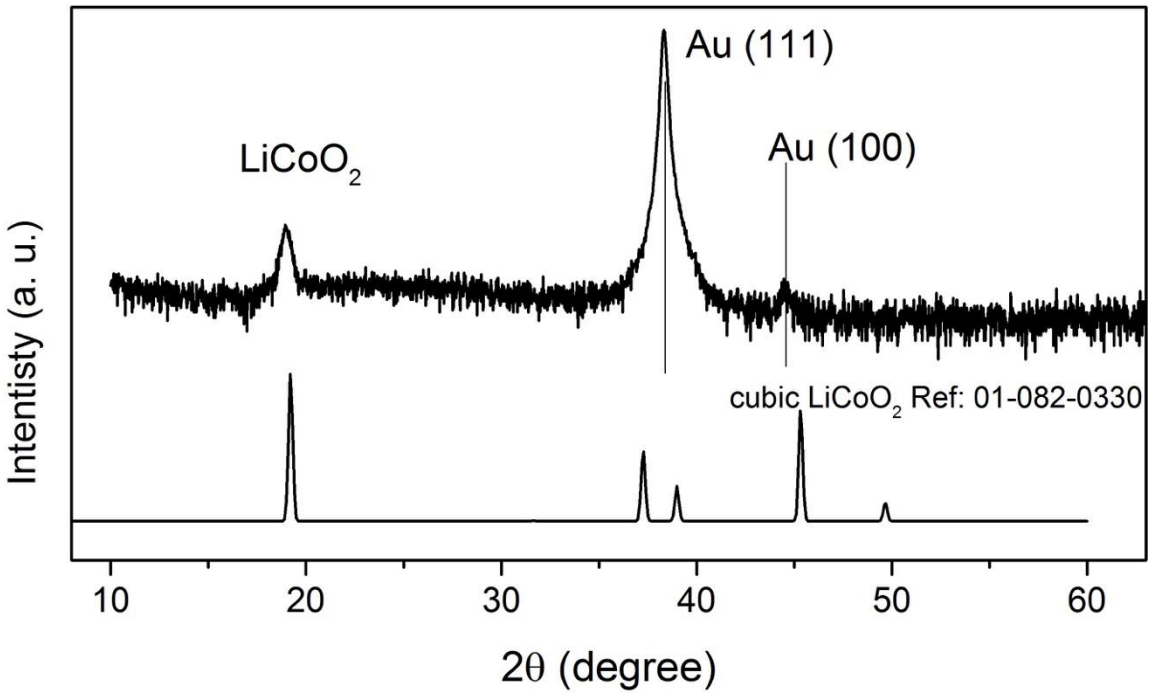

Figure 2. Thin film $LiCoO_2$ X-ray powder diffraction pattern compared to a cubic $LiCoO_2$ reference.

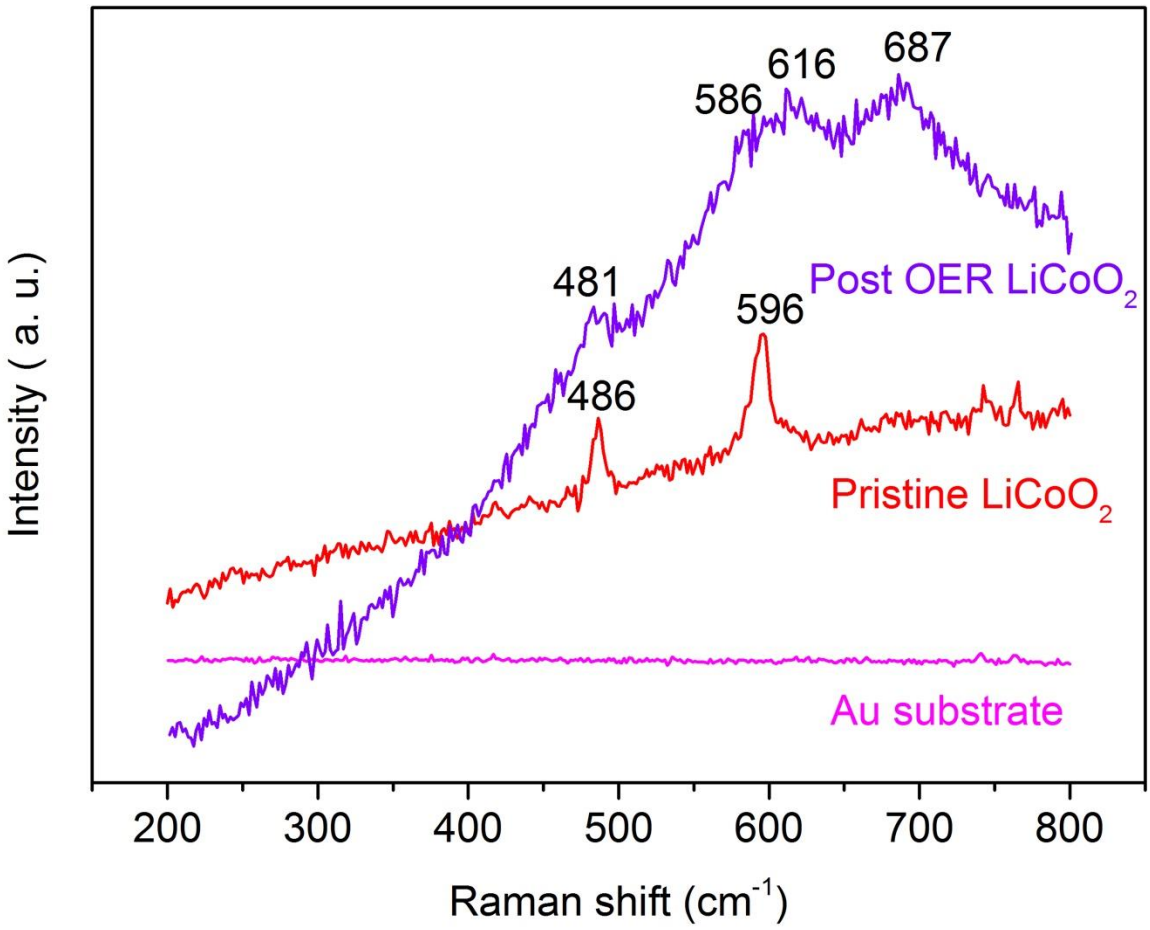

Figure 3. Raman spectra of thin film $LiCoO_2$ (pristine), post-OER-electrolysis $LiCoO_2$ thin film, and Au substrate for comparison.

(A)

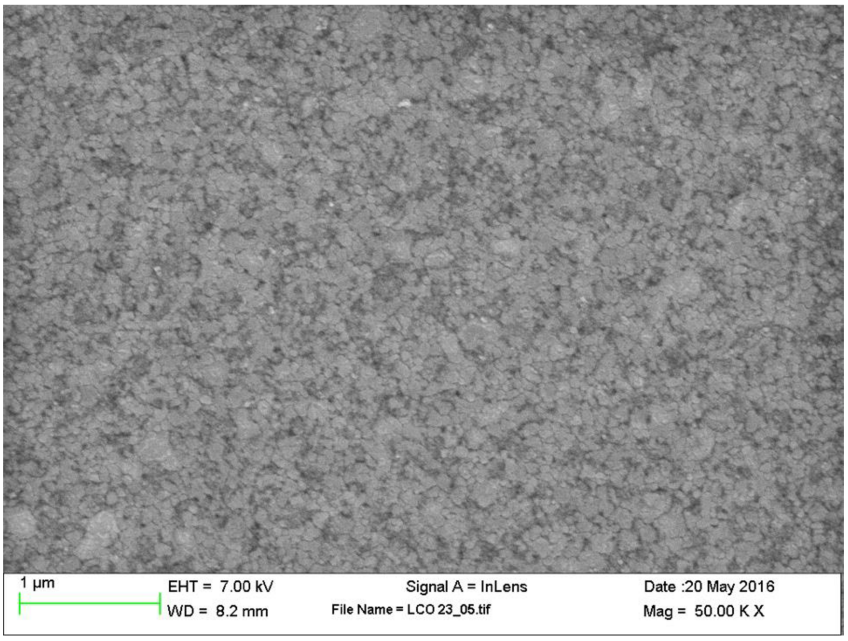

(B)

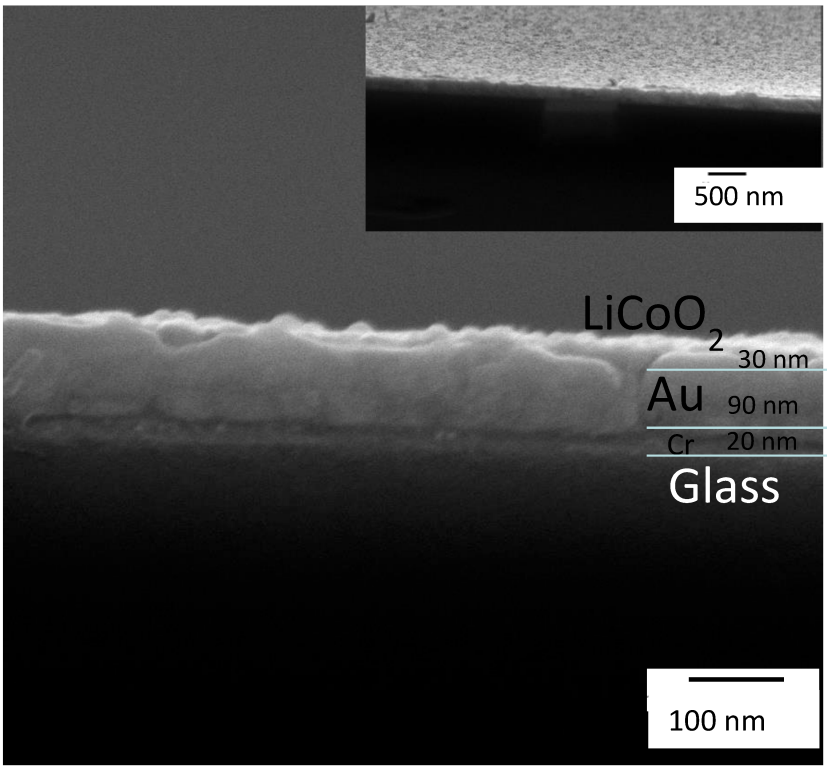

Figure 4. A) a SEM top-view and B) cross-sectional image of thin film $LiCoO_2$, with a canted intermediate-view (inset).

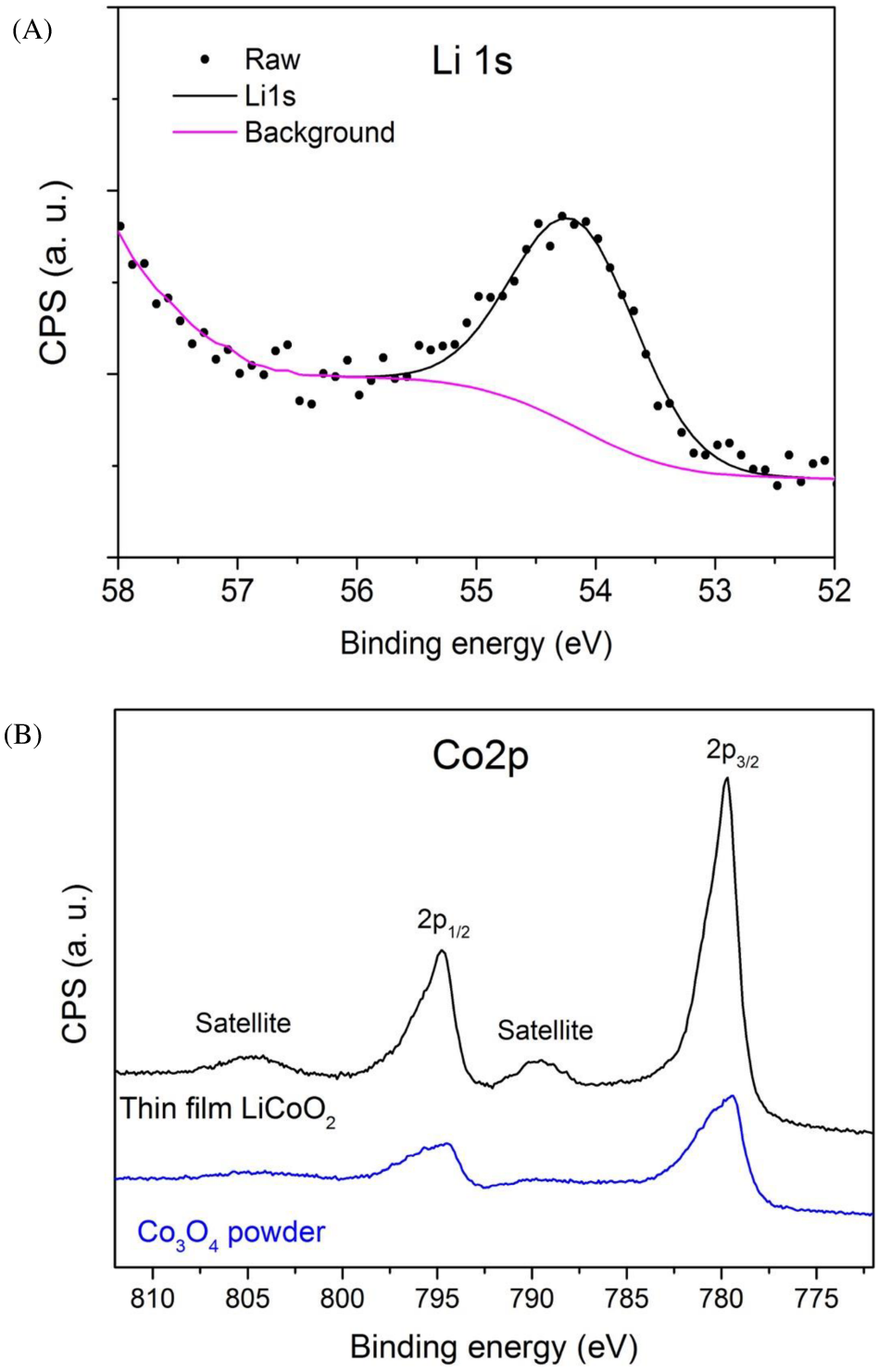

Figure 5. XPS core level photoemission spectrum of A) Li 1s and B) Co 2p for the thin film $LiCoO_2$ compared to Co_3O_4 powder.

(A) (B)

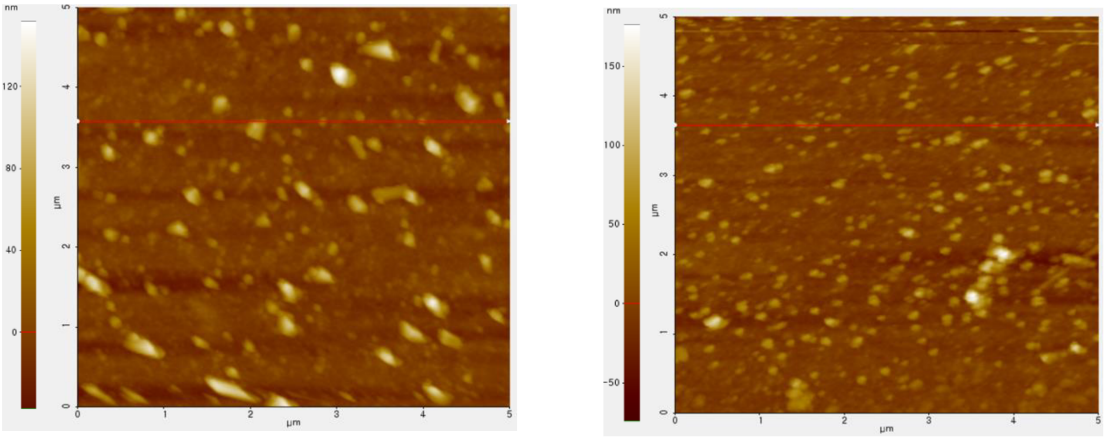

Figure 6. An AFM image of A) a pristine $LiCoO_2$ film, and B) a 12h-cycled $LiCoO_2$ film

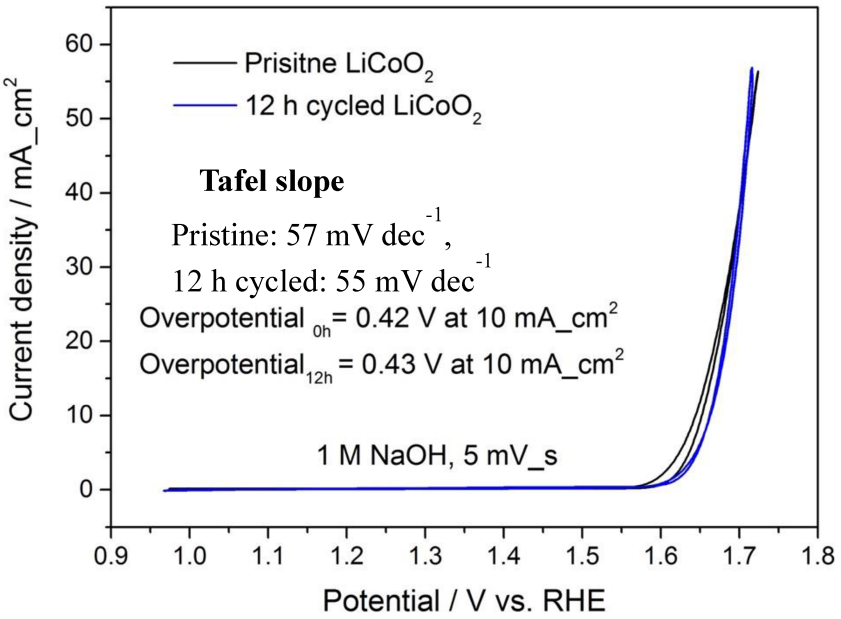

Figure 7. Cyclic voltammograms of thin film $LiCoO_2$ pristine sample and 12h cycled sample in 1 M NaOH.

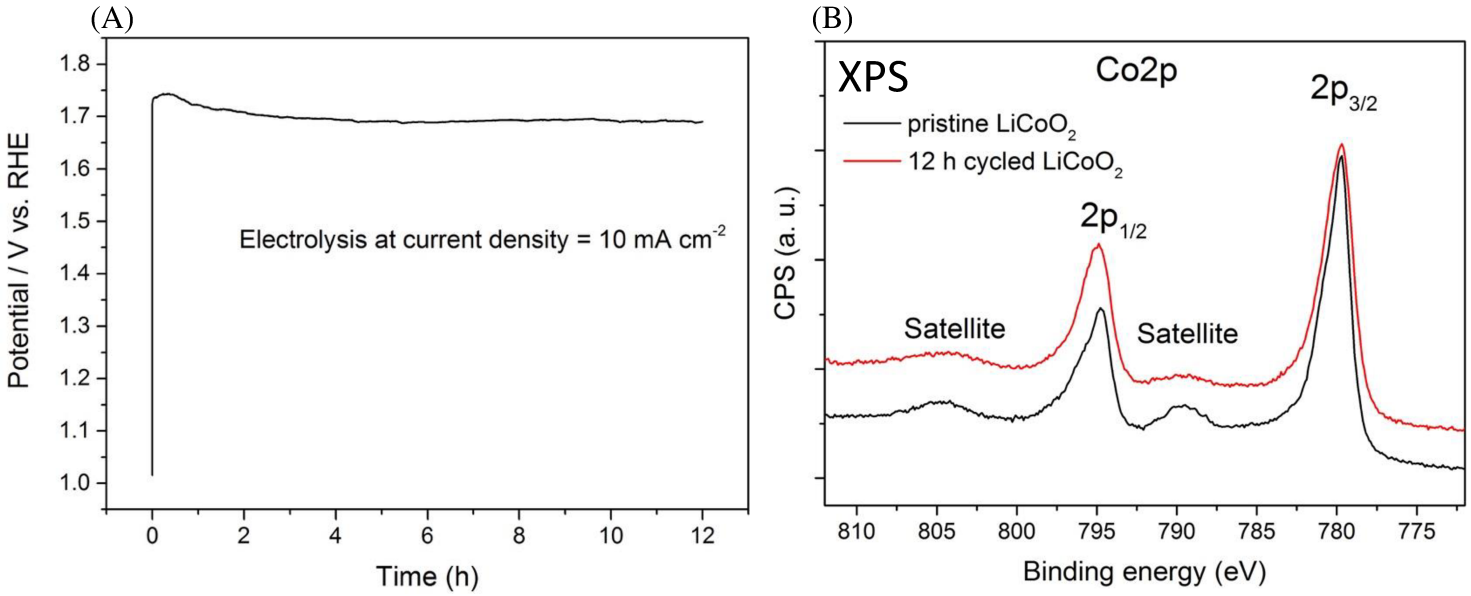

Figure 8. A) Chronopotentiometric electrolysis at 10 mA cm^{-2} of thin film $LiCoO_2$, and B) XPS of Co 2p core level for pristine and post-12h-OER samples.

(A) (B)

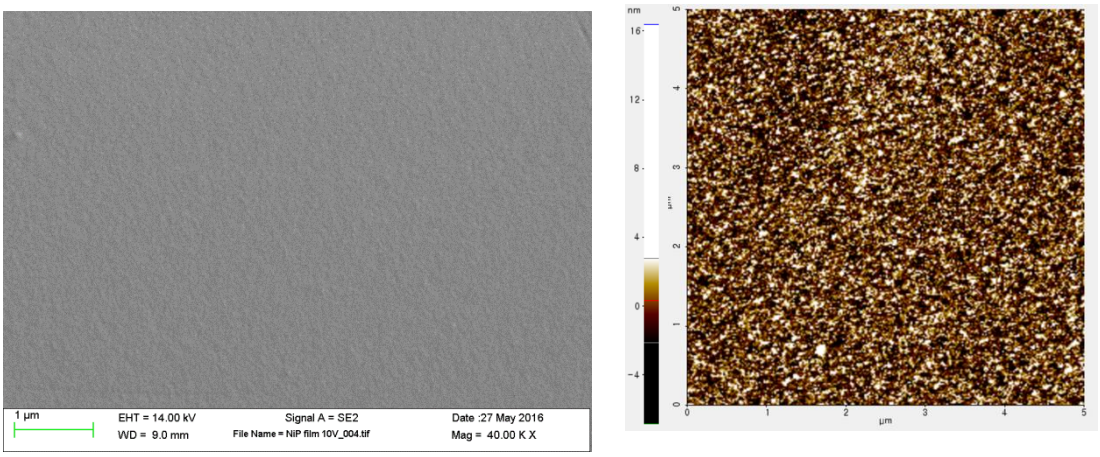

Figure 9. A) SEM of the electrochemically deposited amorphous nickel phosphide morphology, and B) an AFM of Ni-P film exhibiting a roughness (R_a) of 1.7 nm.

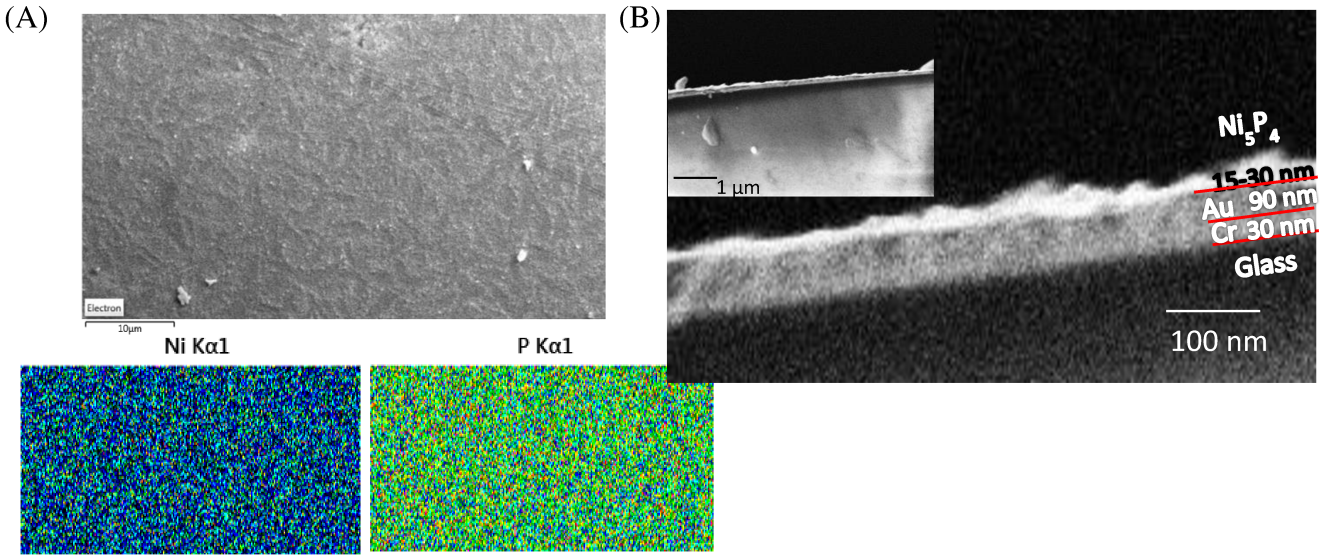

Figure 10. A) a SEM top-view and elemental analysis of Ni_5P_4 thin film by EDS, and B) a cross-section of Ni_5P_4 thin film on an Au/Cr glass substrate.

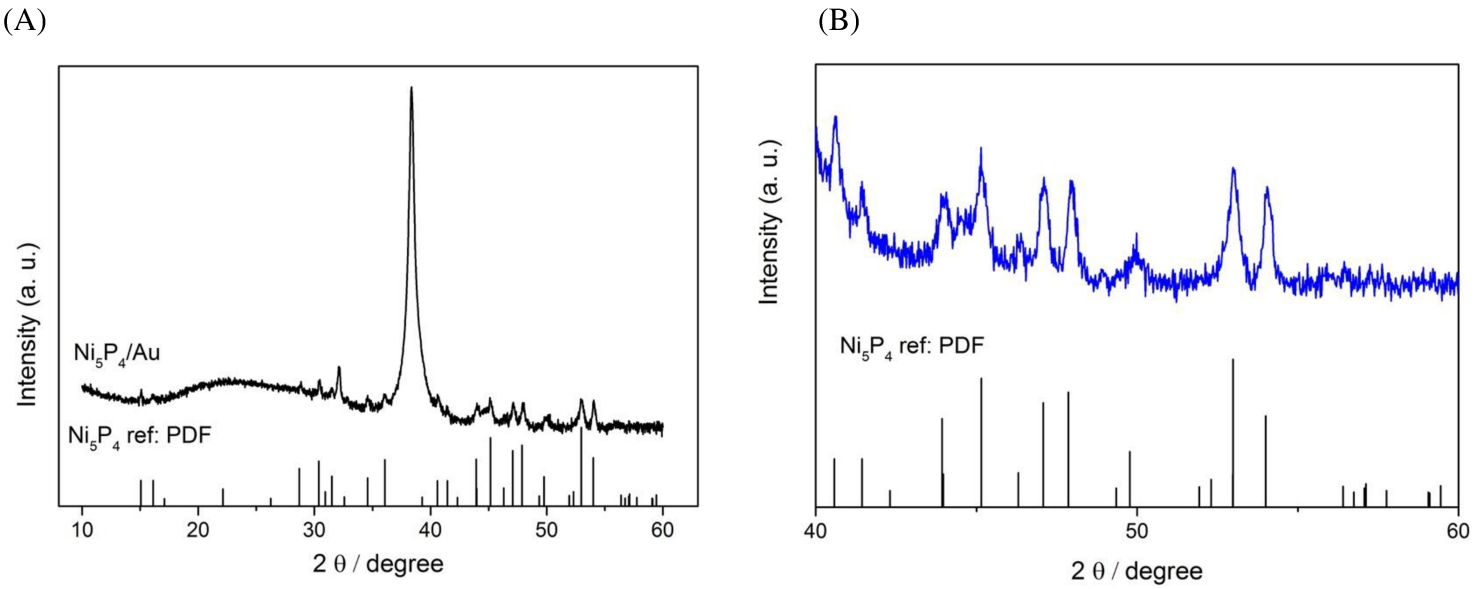

Figure 11. (A) X-ray diffraction pattern of a ~200nm Ni_5P_4 film on Au substrate, and(B) in a range exclusive of the substrate peak.

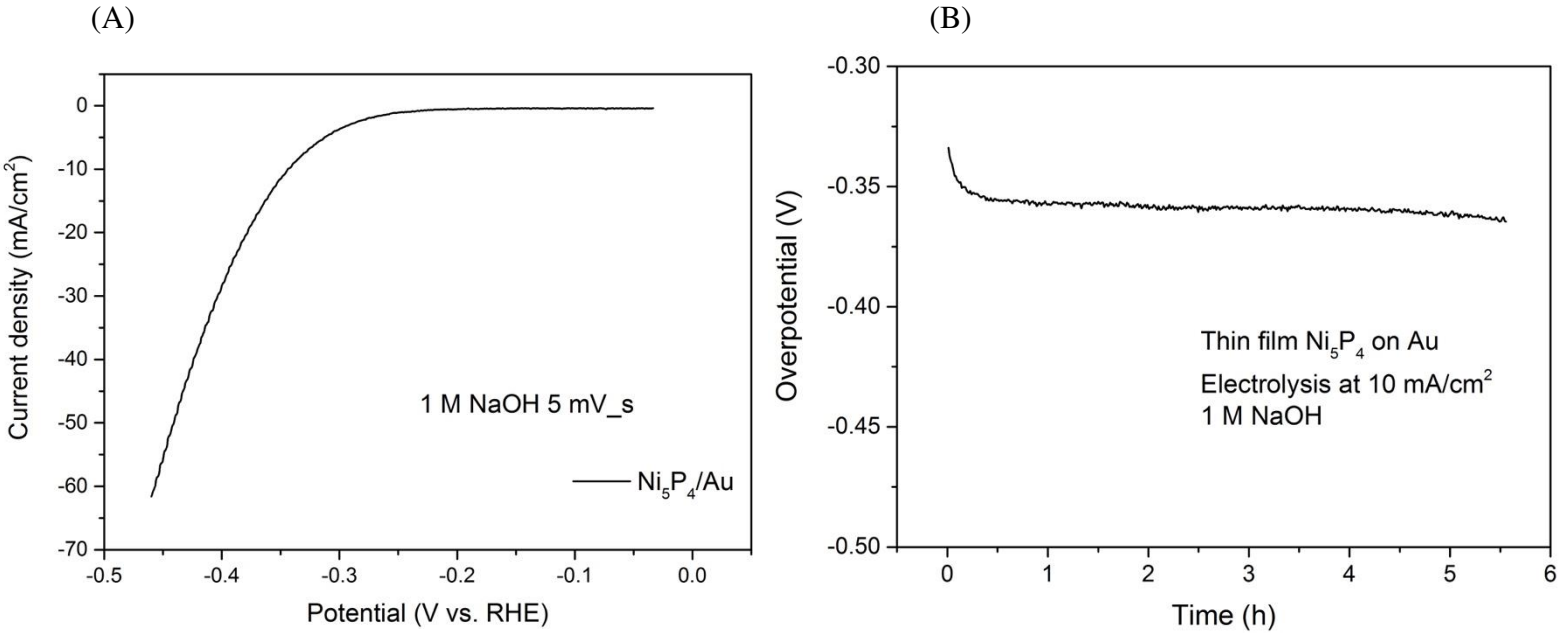

Figure 12. (A) Averaged cyclic voltammogram of the Ni_5P_4 thin film, and (B) chronopotentiometric electrolysis of the Ni_5P_4 thin film at 10 mA/cm^2.

(A) (B)

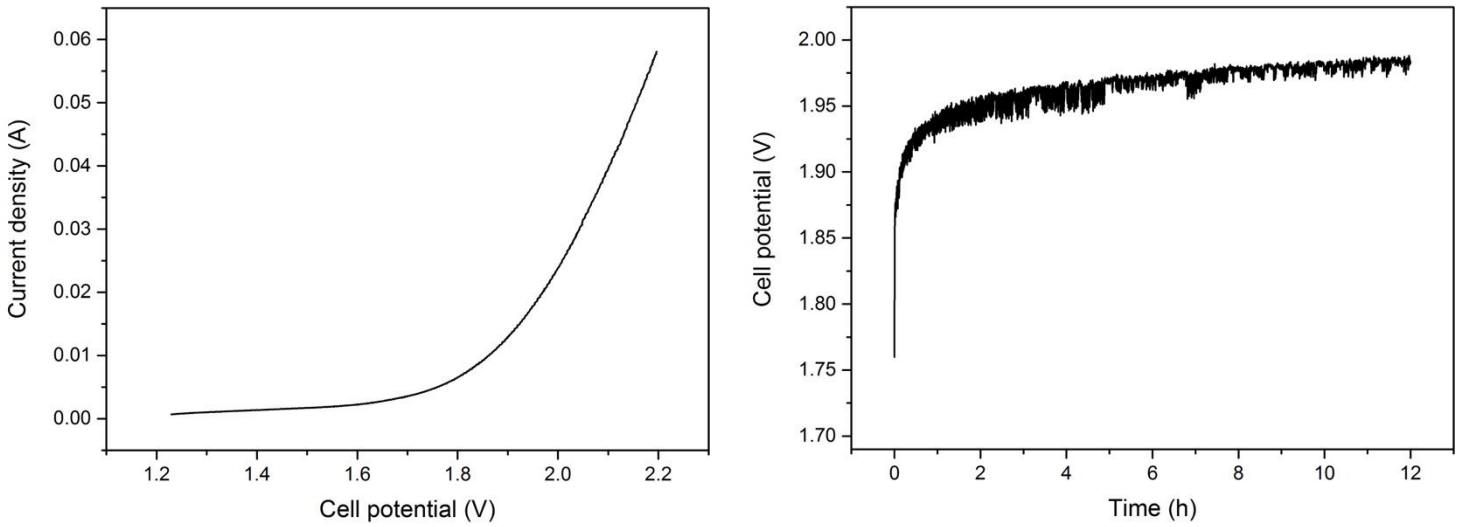

Figure 13. (A) Averaged cyclic voltammogram of overall water splitting, and (B) chronopotentiometric electrolysis of the Ni_5P_4 film (cathode) and $LiCoO_2$ thin film (anode) at 10 mA/cm^2.